



Emergent Spatial Structures in Flocking Models: A Dynamical System Insight

Jean-Baptiste Caussin, Alexandre Solon, Anton Peshkov, Hugues Chaté,
Thierry Dauxois, Julien Tailleur, Vincenzo Vitelli, Denis Bartolo

► To cite this version:

Jean-Baptiste Caussin, Alexandre Solon, Anton Peshkov, Hugues Chaté, Thierry Dauxois, et al..
Emergent Spatial Structures in Flocking Models: A Dynamical System Insight. Physical Review
Letters, 2014, 112, 10.1103/PhysRevLett.112.148102 . cea-01478849

HAL Id: cea-01478849

<https://cea.hal.science/cea-01478849>

Submitted on 28 Feb 2017

HAL is a multi-disciplinary open access archive for the deposit and dissemination of scientific research documents, whether they are published or not. The documents may come from teaching and research institutions in France or abroad, or from public or private research centers.

L'archive ouverte pluridisciplinaire **HAL**, est destinée au dépôt et à la diffusion de documents scientifiques de niveau recherche, publiés ou non, émanant des établissements d'enseignement et de recherche français ou étrangers, des laboratoires publics ou privés.

Emergent spatial structures in flocking models: a dynamical system insight

Jean-Baptiste Caussin,¹ Alexandre Solon,² Anton Peshkov,³ Hugues Chaté,^{4,5,3}
 Thierry Dauxois,¹ Julien Tailleur,² Vincenzo Vitelli,⁶ and Denis Bartolo¹

¹*Laboratoire de Physique de l'Ecole Normale Supérieure de Lyon,
 Université de Lyon, CNRS, 46, allée d'Italie, 69007 Lyon, France*

²*Université Paris Diderot, Sorbonne Paris Cité, MSC, CNRS, 75205 Paris, France*

³*LPTMC, CNRS, Université Pierre et Marie Curie, 75252 Paris, France*

⁴*Service de Physique de l'Etat Condensé, CEA-Saclay, CNRS, 91191 Gif-sur-Yvettes, France*

⁵*Max Planck Institute for Physics of Complex Systems, Nöthnitzer Straße 38, 01187 Dresden, Germany*

⁶*Instituut-Lorenz for Theoretical Physics, Universiteit Leiden, 2300 RA Leiden, The Netherlands*

We show that hydrodynamic theories of polar active matter generically possess inhomogeneous traveling solutions. We introduce a unifying dynamical-system framework to establish the shape of these intrinsically nonlinear patterns, and show that they correspond to those hitherto observed in experiments and numerical simulation: periodic density waves, and solitonic bands, or polar-liquid droplets both cruising in isotropic phases. We elucidate their respective multiplicity and mutual relations, as well as their existence domain.

Could the emergence of collective motion in fish schools, bird flocks, and insect swarms be understood within a unified physical framework? A growing stream of works has approached this provocative question following the seminal work of Vicsek *et al.*, who considered self-propelled point particles interacting solely via local velocity-alignment rules [4]. This model displays a spontaneous rotational-symmetry breaking leading to orientational order [2–4]. In addition, a number of subsequent simulations and experiments have revealed an even more surprising feature. At the onset of collective motion, despite the lack of any attractive interactions, polar active matter self-organizes in the form of band-shape swarms [1, 3, 6–12]. However, depending on the specifics of the systems, these dynamical patterns take three different forms: (i) delocalized density waves [1, 6], as exemplified in Fig. 1a, (ii) solitonic structures [7–9], Fig. 1b, and (iii) phase-separated states [10–12], Fig. 1c. Although it is now clear that they are responsible for the first-order nature of the transition towards collective motion [3, 9, 10], no unifying theory exists to account for the origin and the variety of these band patterns.

In this letter, we convey a comprehensive description of the propagative excitations of polar active matter. Using a hydrodynamic description and dynamical system concepts, we establish the shape of these intrinsically nonlinear band structures, and show that they correspond to those observed in all the available experiments and numerical simulation, see e.g. [1, 6–14].

Our starting point is a hydrodynamic description of compressible polar active fluids [3, 15]. Since we are chiefly interested in structures varying only along the main direction of motion, we focus here on a one-dimensional problem. The local density field $\rho(x, t)$ obeys a conservation equation which complements the equation governing the momentum field $W(x, t) = \rho(x, t)P(x, t)$, where $P(x, t) \in [0, 1]$ is a polarization field. Following

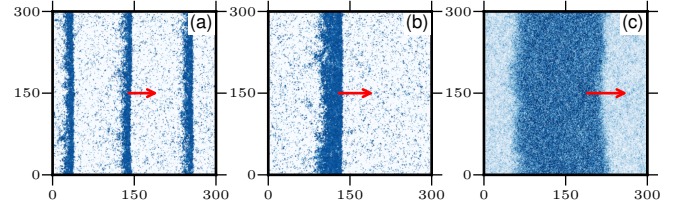


FIG. 1. Band patterns observed in agent-based simulations. (a) Smectic arrangement of polar bands in the Vicsek model with vectorial noise [1]. Speed $v = 0.5$, noise intensity $\eta = 0.6$ and density $\rho = 1.1$. (b) A solitary band observed for the same model and same parameters as in (a). (c) Polar-liquid droplet in an isotropic phase observed in the active Ising model [10], with inverse temperature $\beta = 6$, density $\rho = 5$, hopping rate $D = 1$, and bias $\epsilon = 0.9$. More simulation details can be found in [22].

Toner and Tu [15] these equations read

$$\partial_t \rho + \partial_x W = 0 \quad (1)$$

$$\partial_t W + \xi W \partial_x W = a_2 W - a_4 W^3 - \lambda \partial_x \rho + D \partial_{xx} W \quad (2)$$

where all the coefficients *a priori* depend both on ρ and W^2 . These phenomenological equations were introduced to account for a continuous mean-field transition from a homogeneous isotropic state with $\rho = \rho_0$ and $P = 0$ when $a_2 < 0$, to a homogeneous polarized state with $P = \rho_0^{-1} \sqrt{a_2/a_4}$ when $a_2 > 0$. In addition, the λ term reflects the pressure gradient induced by density heterogeneities. ξ and D are two transport coefficients associated respectively with the advection and the diffusion of the local order parameter. Following [7], we now look for propagating solutions of Eqs. (1) and (2): $\rho = \rho(x - ct)$ and $W = W(x - ct)$, where c is the propagation speed [7, 11]. This ansatz reduces Eq. (1) to an

algebraic relation:

$$\rho = \rho^* + \frac{1}{c}W \quad (3)$$

When a band moves in an isotropic gas, see e.g. Fig. 1b, the constant ρ^* corresponds to the gas density. Inserting the latter expression in Eq. (2) leads to a second order ordinary differential equation:

$$D\ddot{W} + \dot{W} \frac{dF}{dW} + \frac{dH}{dW} = 0, \quad (4)$$

where $H(W)$ is defined via $dH/dW = a_2W - a_4W^3$, $F(W) = (c - \frac{\lambda}{c})W - \frac{1}{2}\xi W^2$, and the dot symbol denotes derivative with respect to $\tau \equiv x - ct$. Therefore, the band-pattern problem is recast into a dynamical system framework: establishing the shape of the bands amounts to describing the motion of a particle of mass D and position W in a potential $H(W)$, and experiencing a non-linear friction $F(W)$, see Fig. 2a. Note that the particle gains (resp. losses) energy when $F'(W) < 0$ (resp. $F'(W) > 0$).

Mass conservation in the original problem, Eq. (1), constrains the boundary conditions of Eq. (4) as $W(x \rightarrow -\infty) = W(x \rightarrow +\infty)$. Given this simple observation, without any further calculation, we can anticipate all the possible band patterns: the solutions of Eq. (4) correspond to closed trajectories in the (W, \dot{W}) plane. Therefore they necessarily belong to one of the three following classes: (i) periodic orbits, (ii) homoclinic cycles (the trajectory includes one saddle point), or (iii) heteroclinic cycles (the trajectory includes two saddle points). Back in real space, as exemplified in Fig. 3, these trajectories respectively correspond to three possible propagating patterns $W(x - ct)$: (i) a smectic phase composed of ordered bands (W varies periodically with $x - ct$), (ii) a localized solitary wave, the length of which being set by the "time" taken to explore the homoclinic cycle, (iii) a polar-liquid droplet separated by domain walls from an isotropic gaseous phase, the fraction of polar liquid being given by the ratio between the waiting times at the two saddle points. These three patterns exactly correspond to those *hitherto* observed in model experiments, and in numerical simulations at the onset of collective motion.

Motivated by this pivotal observation, we now turn to the study of equation (4). For sake of clarity we henceforth specify the functional dependence of the phenomenological coefficients in Eq. (2). As the density is a control parameter of the transition to collective motion for all models based on short-range alignment interactions, $a_2(\rho)$ has to change sign at a finite density ρ_c [2, 3]. Different systems may result in different functions $a_2(\rho)$. We choose a simple linear dependence $a_2 = \rho - \rho_c$ which is consistent, close to ρ_c , with all existing kinetic theories [7, 8, 10, 17, 20]. In addition, having e.g. the original Vicsek model in mind, we want to capture the saturation of the average polarization of a homogeneous polar state

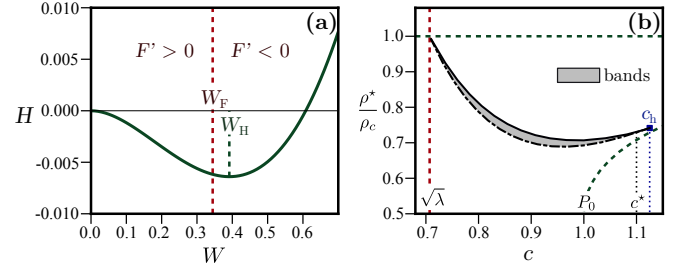


FIG. 2. (a) Sketch of the motion of an oscillating point particle in the effective potential $H(W)$ for $P_0 = 1$, $\rho_c = 1$, $\lambda = 0.5$, $\xi = 1$, $c = 0.9$ and $\rho^* = 0.7$. The system loses or gains energy H when $F'(W) > 0$ or $F'(W) < 0$. (b) Band phase diagram for the same parameters. Non-linear bands exist only in the grey region. The dashed lines correspond to the conditions $W_H > 0$, and $W_F > 0$. For $c < c^*$, the black full line corresponds to the supercritical Hopf-bifurcation. Polar-liquid droplets states are observed only at $c = c_h$.

of density $\rho = \rho_0$, when $\rho_0 \gg \rho_c$, at a non-zero value P_0 . In agent-based models, P_0 is set by the noise amplitude. Here, since $P \sim \rho_0^{-1}[(\rho_0 - \rho_c)/a_4]^{1/2}$, the simplest possible choice yielding the correction saturation is $a_4(\rho) = (\rho P_0^2)^{-1}$. This choice simplifies the equations studied numerically in [11]. In all that follows, ξ , λ and D are kept constant.

Now that Eqs. (1)-(2) have been fully defined, we can obtain their propagative solutions explicitly by solving Eq. (4). We stress that the two functions $H(W)$ and $F(W)$ are parametrized by two independent parameters: ρ^* and c , which specify the shape of the bands. Their explicit form are provided in [22] and H is plotted in Fig. 2a for a given set of parameters. The existence of closed trajectories in the (W, \dot{W}) plane requires that the system has at least one fixed point [19]. Hence, keeping in mind that Eq. (4) describes the motion of a massive particle in a potential, we look for trajectories that display at least one oscillation. This obviously requires: (i) that H has a local minimum at a finite value $W_H > 0$ (and thus a local maximum at $W = 0$), and (ii) that the friction $F'(W)$ changes sign at a finite $W_F > 0$ so that the particle do not fall to and remains stuck at W_H where H is minimum. It is straightforward to show that the former condition implies $\rho^* < \rho_c$, and the latter $c > \sqrt{\lambda}$. In order to establish the shape of the periodic trajectories of the dynamical system, and in turn the shape of the bands, we need to go beyond this simple picture. We introduce the auxiliary variable $Z \equiv D\dot{W} + F(W)$ and recast Eq. (4) into the 2-dimensional dynamical system:

$$\dot{W} = \frac{1}{D} [Z - F(W)] \quad (5)$$

$$\dot{Z} = -\frac{dH}{dW} \quad (6)$$

This change of variable greatly simplifies the investigation of the fixed points of the dynamical system now

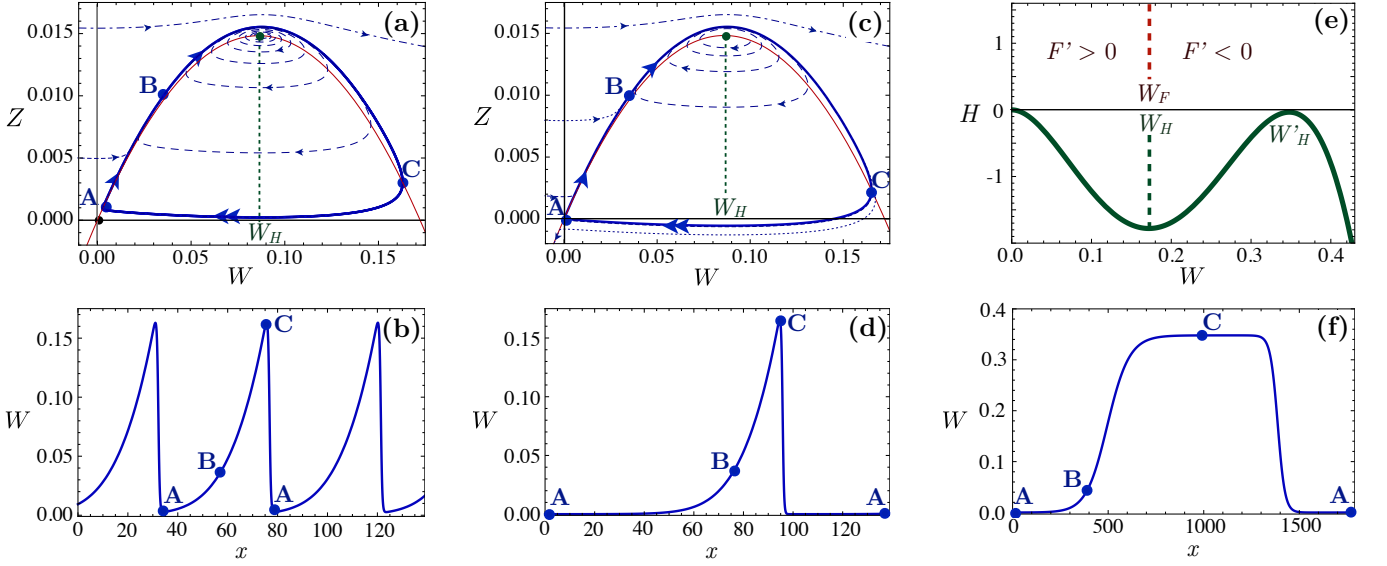


FIG. 3. (a) Dashed lines: dynamical system trajectories, for $P_0 = 1$, $\rho_c = 0.1$, $\lambda = 0.5$, $\xi = 4$, $D = 0.1$, $c = 0.9$. ρ^* was chosen such that $W_H \gtrsim W_F$. Thick line: stable limit cycle. Thin line: $Z = F(W)$ curve. (b) Polar smectic corresponding to the limit cycle shown in (a). (c) Homoclinic orbit; same parameters as in (a) but for a lower value of ρ^* . (d) Solitonic band corresponding to the limit cycle shown in (c). (e) $H(W)$, full line, plotted for $P_0 = 1$, $\rho_c = 1$, $\lambda = 1$, $\xi = 10$ and $D = 50$. The dashed lines show the positions of W_F and W_H . The values of c and ρ^* give rise to an heteroclinic cycle [22]. (f) Polar-liquid droplet for the same values of the parameters as in (e), see also [22].

defined by Eqs (5)-(6) [21]. It has at least two fixed points: $(0, 0)$ and $(W_H, F(W_H))$. A conventional linear stability analysis shows that $(0, 0)$ is always a saddle point. Conversely the second fixed point $(W_H, F(W_H))$ calls for a more careful discussion. It undergoes a Hopf-bifurcation as $W_H - W_F$ changes sign, as can be seen on the eigenvalues of the Jacobian matrices [22]. This bifurcation, which we will thoroughly characterize elsewhere [23], is supercritical (resp. subcritical) if $c < c^*$ (resp. $c > c^*$), where the critical velocity c^* is defined implicitly by $H'''(W_H) = 0$. Both the bifurcation line and c^* can be computed analytically and are shown in Fig. 2b. More importantly, regardless of its sub- or super-critical nature the Hopf bifurcation results in an unstable spiral trajectory which can lead the system towards a cyclic attractor. We now describe how these limit cycles are explored in the (W, Z) plane, and relate these nonlinear trajectories to the morphologies of the band patterns.

Polar smectic phase/periodic orbits. To gain more quantitative insight, we consider large-amplitude cycles in the limit of small D [27]. For small W , Eq. (5) implies that the system quickly relaxes towards the curve $Z = F(W)$ in a time $\sim D^{-1}$. Close to the origin, the dynamics is controlled by the linear properties of the saddle point $(0, 0)$, which defines two well-separated scales. It can be easily shown that the stable direction is nearly horizontal, it is associated with a fast relaxation at the rate $\tau_-^{-1} \sim D^{-1}(c - \lambda/c)$. Conversely, the unstable direction is nearly tangent to the curve $Z = F(W)$, and

corresponds, again in the small- D limit, to a much slower growth at the rate $\tau_+^{-1} \sim (\rho_c - \rho^*)/(c - \lambda/c)$. The shape of large-amplitude cycles immediately follows from this discussion and from the parabolic shape of $F(W)$. Let us start from the left of the cycle, point A in Fig. 3a, close to the origin. We call W_{\min} the abscissa of this point, which is the minimum value of W in the cycle. As noted above, the trajectory first remains near the parabola $Z = F(W)$. If A is close enough to the origin, this part of the cycle is explored slowly, in a time $\sim \tau_+$. Then the trajectory approaches the unstable point $(W_H, F(W_H))$. It therefore leaves the parabola and starts spiraling, at a point labeled B in Fig. 3a (B is here defined as the point where the trajectory deviates from the $Z = F(W)$ curve by 5%). It finally crosses the parabola again, at point C, and W changes sign, see Eq. (5). W then decreases and the system quickly goes back to point A in a time typically set by $\sim \tau_-$. To further check this picture we have numerically computed the phase portraits of Eqs. (5) and (6), Fig. 3a (dotted lines). The typical periodic orbit shown in Fig. 3a (full line) is in excellent agreement with the scenario described above. From this analysis, we infer the shape of the steadily propagating band pattern $W(x - ct)$. As anticipated, periodic orbits correspond to a polar smectic phase composed of equally-spaced bands, in qualitative agreement with the experimental pictures reported in [6], and Fig. 1a. The numerical shape of a smectic pattern is shown in Fig. 3b. It is composed of strongly asymmetric excitations, which reflects the time-scale separation

in the underlying dynamical system close to the origin; the large-amplitude bands are composed of a long exponential tail, and of a sharp front at the head. Note that we describe here the propagation of large-amplitude excitations in a polarized environment. However the minimum polarization in the regions separating the bands, W_{\min} , can be vanishingly small. In this limit the period of the crystalline structure would diverge logarithmically as $\tau_+ \log(W_F/W_{\min})$.

Solitary bands/Homoclinic cycles. In the limiting case where the minimal value of W goes to 0 ($W_{\min} = 0$), point A then corresponds to the saddle located at the origin. Consequently the orbits followed by the dynamical system become homoclinic. As exemplified in Fig. 3c, they are not periodic anymore, as the trajectory remains stuck at $(0, 0)$. In real space, the associated pattern is a solitary wave emerging out of a disordered gas, Fig. 3d. We stress that the existence of solitonic structures at the onset of collective motion is one of the more robust observations made in agent-based simulations [1, 7, 9], see Fig. 1b.

Polar liquid droplets/Heteroclinic cycles. Until now, we have restricted our analysis to the case where the dynamical system only probes the first two extrema of H . However, looking for high-speed solutions ($c > P_0$), H displays an additional extremum at $W'_H > W_H$, see Fig. 3e. $(W'_H, F(W'_H))$ is a second saddle point. Therefore heteroclinic cycles are found when A is located at the origin and C at the second saddle. The cycles are not periodic as the dynamics freezes both at A and C. In real space, the corresponding structure, $W(x - ct)$, is a localized domain, a polar-liquid droplet, traveling in a disordered gas, whose length is given by the residence at point C, Fig. 3f. This phase-separation pattern corresponds to the one numerically observed in the active spin model, Fig. 1c, and in a generalization of the 2D Toner and Tu model [10, 12]. In the small P_0 limit, the shapes of the asymmetric domain walls bounding the polar-liquid droplets can be computed exactly [22].

Several comments are in order. Firstly, we emphasize that the salient features of the swarming patterns do not depend on the specific functional forms of the hydrodynamic coefficients in Eq. (2). The limit-cycle solutions solely require the existence of a Hopf bifurcation, and the dynamics along this cycle is chiefly controlled by the stability of the other fixed points. Therefore, at a qualitative level, only the global shapes of the effective potential $H(W)$ and the friction curve $F(W)$ matter. For instance, we shall stress that a hydrodynamic theory where $a_4 = \text{cst}$ in Eq. (2) would yield non-linear patterns qualitatively identical to those shown in Fig. 1 (not shown). Only the sign reversal of $a_2(\rho)$ at ρ_c was necessary to observe band patterns, in agreement with [16].

Secondly, we emphasize that travelling band can exist when the average density ρ_0 is smaller than ρ_c , though the linear stability of Eqs. (1) and (2) predicts that no

small-amplitude wave can propagate [3]. The fundamental propagative excitations of polar active matter are intrinsically nonlinear below ρ_c .

Thirdly, we come back to the status of the solutions described above. Until now we have identified an infinite family of band-type solutions, located in the vicinity of the Hopf-bifurcation line in the (c, ρ^*) plane, grey region in Fig. 2b. The boundaries of this region are found by looking for non-degenerate solutions satisfying $W > 0$ [23], and its extent is an increasing function of the diffusivity D . The domain of existence of the bands collapses on the Hopf-bifurcation line in the limit $D \rightarrow 0$. The homoclinic cycles, corresponding to solitary waves, are constraint to include one saddle point. Therefore they define a one-parameter ensemble of band-type solutions. This ensemble corresponds to the lower boundary of the phase diagram, Fig. 2b (dashed-dotted line), and is established by taking the infinite-period limit. The heteroclinic solution, polar-liquid droplet, is constrained by the existence of two saddles along a cycle. Therefore, if any, the heteroclinic cycle is unique. It is a limiting case of the one-parameter homoclinic family, point c_h in Fig. 2b.

Finally, we discuss the pattern-selection problem. The ensemble of band-type solutions described above is actually restrained by the mass-conservation law. The mean density ρ_0 in the system is fixed, therefore only band shapes compatible with this value exist. However, we are a priori left with an infinite family of solutions, which is parametrized by one free parameter. Hence, we predict that, for a given value of ρ_0 , several solutions propagating at different speeds may coexist. This conjecture is again supported by numerical evidences. In Fig. 1 the three-band and single-band patterns correspond to identical values of all the simulation parameters. The full resolution of the challenging pattern-selection problem obviously goes beyond the scope of this letter. However, a tentative picture for the nucleation of stationary swarms from a disordered state can be attempted from Eq. (2). The emergence of sharp fronts is natural since the l.h.s. of (2) has the form of Burgers equation, which supports rarefaction shocks [24]. A density fluctuation above ρ_c grows and polarizes via the generic coupling between density and order embodied in the ρ -dependence of a_2 in Eq. (2). When these two competing effects balance each other, the density at the top of the shock is pinned, and a constant-shape asymmetric band steadily propagates. In the transient regime, we therefore expect several bands to form and collide, until the system reaches one of the possible steady states. This mechanism might favor large-amplitude/fast bands via coalescence events, in agreement with the experiments reported in [8].

To close this letter we comment on the role of fluctuations on the transition towards collective motion [2]. Eq. (2) predicts a second-order transition for homogeneous systems. Here, we have evidenced that sta-

tionary polarized excitations (solitary bands, and polar-liquid droplets) can coexist with a homogeneous isotropic phase, which in turn confirms the first order scenario evidenced in numerical simulations [1, 3]. This coexistence does not rely on any fluctuation-induced mechanism, unlike all the conventional equilibrium scenarios making first order a mean-field second-order transition (e.g. Brazovskii [25] and Halperin-Lubensky-Ma [26]). However, beyond the mean-field deterministic picture, fluctuations are very likely to play a major role in the stability, the selection, and the ordering of the band patterns. These difficult but crucial problems are the topic for future work.

We thank J. Toner for valuable comments and suggestions. DB acknowledges support from Institut Universitaire de France, and ANR project MiTra. HC, AP, AS, and JT thank the Max Planck Institute for the Physics of Complex Systems, Dresden, for providing the framework of the Advanced Study Group “Statistical Physics of Collective Motion” within which part of this work was performed.

-
- [1] T. Vicsek, A. Czirók, E. Ben-Jacob, I. Cohen, and O. Shochet, *Phys. Rev. Lett.* **75**, 1226 (1995)
 - [2] T. Vicsek and A. Zafeiris, *Physics Reports* **517**, 71 (2012)
 - [3] M.C. Marchetti, J.F. Joanny, S. Ramaswamy, T. B. Liverpool, J. Prost, M. Rao, and R.A. Simha, *Rev. Mod. Phys.* **85**, 1143 (2013)
 - [4] G. Grégoire, and H. Chaté, *Phys. Rev. Lett.* **92**, 025702 (2004)
 - [5] H. Chaté, F. Ginelli, G. Grégoire, and F. Raynaud, *Phys. Rev. E* **77**, 046113 (2008). H. Chaté, F. Ginelli, G. Grégoire, F. Peruani, and F. Raynaud., *Eur. Phys. J. B.* **64**, 451 (2008)
 - [6] V. Schaller, C. Weber, C. Semmrich, E. Frey, and A.R. Bausch, *Nature* **467**, 73 (2010)
 - [7] E. Bertin, M. Droz, and G. Grégoire, *Phys. Rev. E* **74**, 022101 (2006); *J. Phys A: Math. Theor.* **42**, 445001 (2009)
 - [8] A. Bricard, J.B. Caussin, N. Desreumaux, O. Dauchot, and D. Bartolo, *Nature*, **503**, 95 (2013)
 - [9] T. Ihle, *Phys. Rev. E* **88**, 040303 (2013)
 - [10] A.P. Solon, and J. Tailleur, *Phys. Rev. Lett.* **111**, 078101 (2013)
 - [11] S. Mishra, A. Baskaran, and M.C. Marchetti, *Phys. Rev. E* **81**, 061916 (2010)
 - [12] A. Gopinath, M.F. Hagan, M. C. Marchetti, and A. Baskaran, *Phys. Rev. E* **85**, 061903 (2012)
 - [13] C.A. Weber, T. Hanke, J. Deseigne, S. Léonard, O. Dauchot, E. Frey, and H. Chaté, *Phys. Rev. Lett.* **110**, 208001 (2013)
 - [14] P. Romanczuk, and L. Schimansky-Geier, *Ecological Complexity* **10**, 83 (2012)
 - [15] J. Toner, and Y. Tu, *Phys. Rev. Lett.* **75**, 4326 (1995). J. Toner, Y. Tu, and M. Ulm, *Phys. Rev. Lett.* **80**, 4819 (1998)
 - [16] A. Peshkov, S. Ngo, E. Bertin, H. Chaté, and F. Ginelli, *Phys. Rev. Lett.* **109**, 098101 (2012)
 - [17] F.D.C. Farrell, M.C. Marchetti, D. Marenduzzo, and J. Tailleur, *Phys. Rev. Lett.* **108**, 248101 (2012).
 - [18] T. Ihle, *Phys. Rev. E* **83**, 030901 (2011)
 - [19] V.I. Arnold, *Ordinary Differential Equations* (MIT Press, Cambridge, MA, 1980)
 - [20] A. Baskaran, and M.C. Marchetti, *Phys. Rev. E* **77**, 011920 (2008)
 - [21] S.H. Strogatz, *Nonlinear Dynamics and Chaos* (Addison-Wesley, New York 1994)
 - [22] Supplementary information: details of the simulations of Fig. 1, expressions of H and F , eigenvalues of the Jacobian matrix evaluated at $(W_H, F(W_H))$, and exact expression for the shape of the polar-liquid droplets.
 - [23] A. Solon et al, to be published.
 - [24] G.B. Whitham, *Linear and Nonlinear Waves* (John Wiley & Sons, New York, 1974)
 - [25] S. A. Brazovskii, *Sov Phys JETP* **41**, 85 (1975)
 - [26] B. I. Halperin, T. C. Lubensky, and S.-K. Ma, *Phys. Rev. Lett.* **32**, 292 (1974)
 - [27] More precisely, we consider $D \ll \frac{(c^2 - \lambda)^2}{4c^2(\rho_c - \rho^*)}$.

Supplementary Information

I. MICROSCOPIC MODELS

Figure 1 of the main text shows typical examples of inhomogeneous structures found in polar flocking models. Fig. 1a and 1b stem from a Vicsek model with vectorial noise [1] while Fig. 1c comes from an active Ising model [2]. We recall below the definition of these models, while more details can be found in the original publications [1, 2].

A. Vicsek model

N point-like particles are moving off-lattice in 2d at constant speed v_0 . At each time step, the direction along which each particle moves is updated in parallel, according to the rule

$$\theta_i(t+1) = \arg \left(\sum_{j \in \mathcal{S}_i} \mathbf{v}_j(t) + \eta \mathcal{N}_i \xi \right) \quad (7)$$

where θ_i is the angle made by the velocity \mathbf{v}_i of the i^{th} particle and, say the x -axis. The sum runs on particles in \mathcal{S}_i , the neighborhood of i of radius r_0 . \mathcal{N}_i is the number of particles in \mathcal{S}_i and ξ is a random unit vector with no angular correlation. This equation defines so-called vectorial noise version of the Vicsek model [1, 4].

B. Active Ising model

N particles carrying a spin ± 1 move and interact on a 2d lattice, an arbitrary number of particles being allowed on each site. The particles can hop to any adjacent sites or flip their spins according to Monte-Carlo rates. The spin-flipping results from an on-site ferromagnetic interaction, a particle reverses its spin S on site i at rate

$$W(S \rightarrow -S) = \exp \left(-\beta S \frac{m_i}{\rho_i} \right) \quad (8)$$

where m_i and ρ_i are the magnetization and the number of particles on site i and β plays the role of an inverse temperature. The “self-propulsion” of the particles stems from a bias on the hopping direction: particle k hop to the left (resp. right) with rates $D(1 + \varepsilon S_k)$ (resp. $D(1 - \varepsilon S_k)$) and to the top and bottom with rate D . This sets an effective self-propulsion at speed $2D\varepsilon S_k$ in the horizontal direction.

II. EXPRESSIONS OF H AND F

Using the functional dependences of $a_2(\rho)$ and $a_4(\rho)$ that we introduced in the main text, we find the following expressions for the friction F and the potential H :

$$F(W) = (c - \lambda c^{-1}) W - \frac{1}{2} \xi W^2, \quad (9)$$

$$\frac{dH}{dW} = \left[-(\rho_c - \rho^*) + \frac{W}{c} - \frac{cW^2}{P_0^2(c\rho^* + W)} \right] W. \quad (10)$$

The latter equation can be integrated over W and yields

$$\begin{aligned} H(W) = & -\frac{1}{2}(\rho_c - \rho^*)W^2 + \frac{1}{3c}W^3 - \frac{c^3\rho^{*2}}{P_0^2}W + \frac{c^2\rho^*}{2P_0^2}W^2 \\ & - \frac{c}{3P_0^2}W^3 + \frac{c^4\rho^{*3}}{P_0^2} \log \left(1 + \frac{W}{c\rho^*} \right). \end{aligned} \quad (11)$$

III. EIGENVALUES OF THE JACOBIAN MATRIX

The eigenvalues of the Jacobian matrix evaluated at the fixed point $(W_H, F(W_H))$ are plotted in Fig. 4. The signs of their real and imaginary parts are only set by the difference $W_H - W_F$, hence a Hopf bifurcation occurs at $W_H = W_F$.

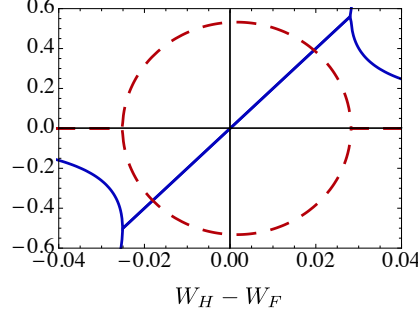


FIG. 4. Eigenvalues of the Jacobian matrix at the fixed point $(W_H, F(W_H))$, as a function of $W_H - W_F$. The curves were plotted for fixed $c = 0.9$ by varying ρ^* . Blue solid line: real part. Red dashed line: imaginary part.

IV. POLAR LIQUID DOMAINS/HETEROCLINIC CYCLES

We compute analytically the shape of the heteroclinic orbits, *i.e.* the boundary between a polar-liquid droplet and the surrounding isotropic gas, in the limit of small P_0 . Since the magnetization scale is set by P_0 , when $P_0 \rightarrow 0$, $W \ll \rho^*$ so that the Hamiltonian reduces to

$$\frac{dH}{dW} = \left[-(\rho_c - \rho^*) + \frac{W}{c} - \frac{W^2}{P_0^2 \rho^*} \right] W \quad (12)$$

Note that this cubic expression becomes exact if we assume the coefficient a_4 to be independent of ρ and W^2 , in the hydrodynamic equations (Eq. (2) main text). With this potential, solutions can be found using the Ansatz

$$W_{\pm}(x - ct) = \frac{W'_H}{2} [1 + \tanh(\Lambda_{\pm}(x - ct))], \quad (13)$$

which yields excellent agreement with the numerical solution of the ODE, see Fig. 5. For a given set of parameters, only one heteroclinic cycle is found in the (ρ^*, c) plane and indeed, inserting Eq. (13) in the ODE with the potential given by Eq. (12) we obtain a unique solution (ρ^*, c) given by

$$c = \frac{1}{3\sqrt{2}} \sqrt{\tilde{P}_0 + 9\lambda + \sqrt{72P_0^2\lambda + (9\lambda + \tilde{P}_0^2)^2}} \quad (14)$$

$$\rho^* = \frac{9c^2\rho_c}{9c^2 + 2P_0^2} \quad (15)$$

$$W'_H = \frac{2P_0^2\rho^*}{3c} \quad (16)$$

$$\Lambda_{\pm} = \frac{(c - \frac{\lambda}{c})}{4D} \left(-1 \pm \sqrt{1 + \frac{4D(\rho_c - \rho^*)}{(c - \frac{\lambda}{c})^2}} \right) \quad (17)$$

where $\tilde{P}_0 = P_0^2(3\xi\rho_c - 2)$. Table I compares the five parameters c , ρ^* , W'_H , Λ_+ and Λ_- found analytically to the best fit. The agreement is excellent.

We thank J. Toner for a careful reading of the supplementary document and for suggesting the compact formula shown in Eq. (16).

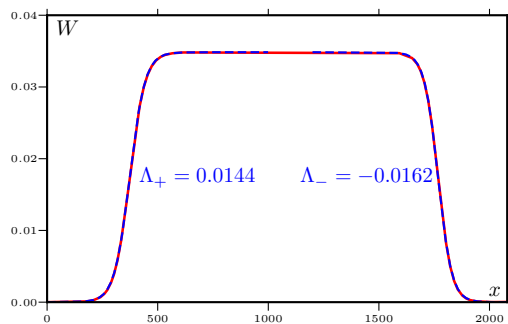


FIG. 5. Heteroclinic orbit obtained by numerical integration (plain red line) and fit with Ansatz (13) (dashed blue lines). Fitting parameters are the width of the front Λ_{\pm} and the position of the front. Parameters: $P_0 = 0.1$, $\rho_c = 1$, $\xi = 10$, $\lambda = 0.01$, $D = 50$, $c = 0.218$, $\rho^* = 0.9502$.

	Numerical	Analytical
c	0.218	0.2041
ρ^*	0.9502	0.949
W'_H	0.0348	0.0310
Λ_+	0.0144	0.0152
Λ_-	-0.0162	-0.0167

TABLE I. Comparison between numerical and analytical values obtained in the limit $P_0 \rightarrow 0$. Parameters: $P_0 = 0.1$, $\rho_c = 1$, $\xi = 10$, $\lambda = 0.01$, $D = 50$. Numerically, Λ_{\pm} are obtained by fitting the profile with Ansatz (13).

-
- [1] H. Chaté, F. Ginelli, G Grégoire, and F. Raynaud, *Phys. Rev. E* **77**, 046113 (2008)
 - [2] A.P. Solon, and J. Tailleur, *Phys. Rev. Lett.* **111**, 078101 (2013)
 - [3] G. Grégoire, and H. Chaté, *Phys. Rev. Lett.* **92**, 025702 (2004)
 - [4] T. Vicsek, A. Czirók, E. Ben-Jacob, I. Cohen, and O. Shochet, *Phys. Rev. Lett.* **75**, 1226 (1995)